New Results in Dielectric-Loaded Resonators

KAWTHAR A. ZAKI, SENIOR MEMBER, IEEE, AND CHUNMING CHEN, STUDENT MEMBER, IEEE

Abstract—**Analysis of cylindrical dielectric-loaded resonators is reviewed. The fields within the dielectric-loaded region are postulated as the superposition of hybrid, TE, or TM modes of the infinite dielectric-loaded waveguide, while the fields in the end regions of the resonators are described by the superposition of the normal modes of a homogeneously filled waveguide. Numerical results are presented which reveal that accurate representation of the fields in the resonant structure generally require several modes. Hence, the resonant modes cannot be correlated directly with single waveguide modes. A new method for mode identification is proposed. For a wide range of parameters, the resonant frequencies, mode charts, field expansion coefficients, field intensity, and distributions are presented. Excellent agreement of the mode charts with resonant frequency measurement results are obtained.**

I. Introduction

THE PURPOSE OF this paper is to review and extend the analysis method described in [1]–[3], and present new numerical results and extensive measured data for the verification of the analysis.

The continuing interest in dielectric resonators for applications in microwave and millimeter-wave systems prompted many researchers to develop and refine analysis methods for the design of such resonators. Modes in isolated resonators with no metallic boundaries have been analyzed extensively using the approximate technique of magnetic wall on all or portions of the resonator's surface [4], [7]. This technique is valid in the limit as the relative dielectric constant of the material approaches infinity. For waveguides and resonators with metallic boundaries, exact closed-form solution methods have been presented for certain geometries [2], [3]; variational and perturbation techniques [8]–[10] have also been used extensively whenever the geometry did not allow closed-form solutions to be developed. Other analysis methods based on field expansions in term of eigenmodes of the resonators and enclosures [1], [11]–[16] and on surface integral equations [17]–[18] have recently been developed.

The method of analysis for accurate determination of the resonant frequencies and field distributions within a circular cylindrical dielectric resonator shielded by a coaxial circular conducting boundary is summarized in Section II. Symmetry conditions are employed to reduce the size of the determinant whose roots are the resonant frequencies by a factor of two. Since the fields in the resonator are expressed as a linear combination of several eigenmodes of the dielectric-loaded waveguide, and no single mode is dominant, designation of the resonant frequencies of the structure cannot be directly correlated with any single waveguide mode. A method for the designation of the resonant frequencies is proposed in Section III.

Extensive numerical results showing the convergence of the solution and "mode charts" for typical resonators are included in Section IV. Mode charts are verified extensively by measurements on several experimental resonators. Variation of the mode coefficients in the dielectric-loaded waveguide and end sections as a function of the resonator parameters are presented.

Section V presents results of several representative plots of the resonator's field distribution and intensity.

II. Method of Analysis

The resonator structure is shown in Fig. 1. The metallic cavity of radius b and length L has perfectly conducting walls. The dielectric cylinder of radius a, relative dielectric constant ϵ_{r1}, and length l is placed symmetrically within the cavity, and is supported by concentric rings of a low relative dielectric constant material ϵ_{r2} (e.g., foam). This support can be conveniently made as two half-cups, between which the resonator is enclosed. Alternatively, the end supports can be of different dielectric constant material ϵ_{r3}. Extensive analysis and numerical results of this structure in the special case of $l = L$ were presented in [3]. Following the reasoning by Kobayashi *et al.* [15], because of the structural symmetry electromagnetic fields existing in the resonator can be classified into two classes: i) fields which have zero transverse electric fields in the symmetry plane $z = 0$ (i.e., electric wall boundary condition at $z = 0$), and ii) fields which have zero transverse magnetic fields in the symmetry plane $z = 0$ (i.e., magnetic wall boundary condition at $z = 0$).

The resonator structure is divided into three regions, A, B, and C as indicated in Fig. 1. Because of the symmetry, only the fields in the region $z \geq 0$ will be considered in the analysis that follows. In region $A(L/2 \geq z \geq l/2)$, the fields are expressed as a linear combination of the normal TE and TM modes of the homogeneously filled circular waveguide of radius b [19]. In region $B(l/2 \geq z \geq 0)$, the fields are expressed as a linear combination of the hybrid, TE or TM modes of the dielectric-loaded waveguide [1],

Manuscript received November 11, 1985; revised February 5, 1986. This material is based upon work supported by the National Science Foundation under Grant ECS-8320249.

The authors are with the Department of Electrical Engineering, University of Maryland, College Park, MD 20742.

IEEE Log Number 8608326.

0018-9480/86/0700–0815$01.00 ©1986 IEEE

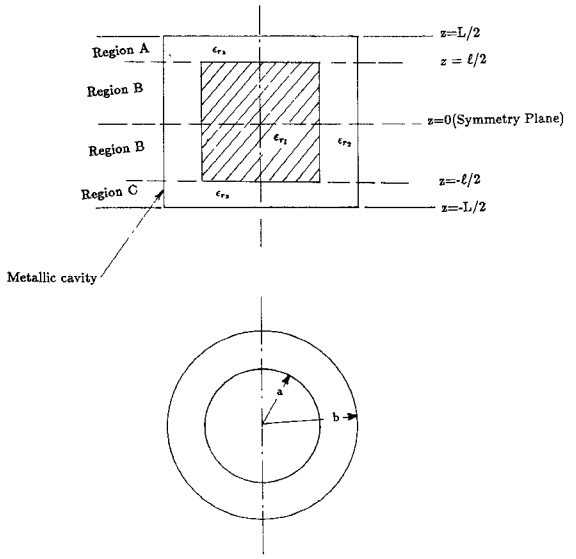

Fig. 1. Dielectric-loaded resonator geometry.

[2]. To satisfy the boundary conditions that the transverse electric and magnetic fields be continuous at the boundary $z = l/2$, it is necessary that the angular variation of the fields be the same in each of the regions A and B. This implies that the resonator fields must belong to one of the following three possible categories:

i) transverse electric (TE) modes in both regions A and B with no angular variation of the fields;
ii) transverse magnetic (TM) modes in both regions A and B with no angular variation of the fields; or
iii) combination of TE and TM modes in region A, and hybrid modes in region B. In both regions, all modes must have the same angular variation (i.e., $\sin n\phi$ and $\cos n\phi$).

The transverse fields in each of the regions A and B which satisfy the boundary conditions of zero tangential electric fields at the end face $z = L/2$, and the zero tangential electric field (electric wall boundary at $z = 0$) or zero tangential magnetic field (magnetic wall boundary at $z = 0$) can be expressed as

$$\bar{E}_A = \sum_j a_j \hat{e}_j \sinh\gamma_j(L/2 - z) \tag{1a}$$

$$\bar{H}_A = \sum_j a_j \hat{h}_j \cosh\gamma_j(L/2 - z) \tag{1b}$$

$$\bar{E}_B = \sum_j A_j \hat{E}_j \begin{pmatrix} -\sinh\Gamma_j z \\ \cosh\Gamma_j z \end{pmatrix} \tag{1c}$$

$$\bar{H}_B = \sum_j A_j \hat{H}_j \begin{pmatrix} \cosh\Gamma_j z \\ -\sinh\Gamma_j z \end{pmatrix} \tag{1d}$$

where γ_j, $\hat{e}_j$, and $\hat{h}_j$ are propagation constants, transverse electric and magnetic fields of the normal TE and TM modes in the homogeneously filled waveguide of radius b, respectively; Γ_j, $\hat{E}_j$, $\hat{H}_j$ are propagation constants, transverse electric and magnetic fields of the (hybrid) modes in the dielectric-loaded waveguide, respectively. The upper and lower values in the equations (1c) and (1d) correspond to electric and magnetic wall conditions in the symmetry plane $z = 0$, respectively. Expressions for these fields and the characteristic equation whose roots are the Γ_i's can be found in [2]. All the modes in (1) have the same angular variation, thus the summation on j is a single sum corresponding to the various radial variations of the wave numbers.

Expressions (1c) and (1d) are valid, since (it is conjectured that) the hybrid-mode fields ($\hat{E}_j$, $\hat{H}_j$) form a complete set over the dielectric-loaded waveguide's cross section. Although Clarricoats and Taylor [20] predicted the existence of complex propagation constants Γ_j for certain combinations of the physical parameters of the dielectric-loaded waveguide, in this paper, based on physical reasoning, that growing waves could not exist in a passive structure, only purely real or purely imaginary roots of the characteristic equation were sought and found in the numerical solution. No attempts have been made to investigate the existence, or use of, the complex modes in the field expansions. The boundary conditions to be satisfied by the fields of (1) are that the transverse electric and magnetic fields be continuous at $z = l/2$

$$\bar{E}_A = \bar{E}_B; \quad \bar{H}_A = \bar{H}_B \qquad \text{at } z = l/2. \tag{2}$$

Taking the dot product of the electric-field equation with $\hat{e}_i^*$ and the magnetic-field equation with $\hat{h}_i^*$ and integrating over the guide cross section S, using the orthogonality properties of the normal waveguide modes [19], the following set of homogeneous equations results:

$$a_i\langle\hat{e}_i, \hat{e}_i\rangle s_i = \sum_j Aj\langle\hat{E}_j, \hat{e}_i\rangle \begin{pmatrix} -S_j \\ C_j \end{pmatrix} \tag{3a}$$

$$a_i\langle\hat{h}_i, \hat{h}_i\rangle c_i = \sum_j Aj\langle\hat{H}_j, \hat{h}_i\rangle \begin{pmatrix} C_j \\ -S_j \end{pmatrix} \tag{3b}$$

where

$$\langle\hat{u}_i, \hat{v}_j\rangle = \int_s \hat{u}_j \cdot \hat{v}_j^* ds$$

$$s_i = \sinh\gamma_i(L - l/2), \quad S_j = \sinh\Gamma_j l/2$$

$$c_i = \cosh\gamma_i(L - l/2), \quad C_j = \cosh\Gamma_j l/2.$$

Closed-form expressions for the inner products in (3) are given in the Appendix. The a_i's can be eliminated from (3a) and (3b), leaving a homogeneous system of equations in A_j's only

$$\sum_j X_{ij} A_j = 0 \tag{4}$$

where

$$X_{ij} = \frac{\langle\hat{E}_j, \hat{e}_i\rangle}{\langle\hat{e}_i, \hat{e}_i\rangle} c_i \begin{pmatrix} -S_j \\ C_j \end{pmatrix} - \frac{\langle\hat{H}_j, \hat{h}_i\rangle}{\langle\hat{h}_i, \hat{h}_i\rangle} s_i \begin{pmatrix} C_j \\ -S_j \end{pmatrix}. \tag{5}$$

The resonant frequencies of the structure are the roots of the equation

$$\det[X] = 0 \tag{6}$$

where the element values of the matrix X i.e., (X_{ij}) are given by (5). Numerical solution of (6) is accomplished by truncating the infinite matrix X to finite size $N = 2p$. The modes are chosen as follows: for nonaxially symmetric fields in region A, p-TE modes and p-TM modes, while in region B, $2p$ hybrid modes. Thus, there will be $2p$ unknowns (A_j)'s for the hybrid mode coefficients, and $2p$ equations corresponding to the normal TE and TM modes. For the case of no ϕ-variation, p TE (or TM) modes are chosen in region A and p TE (or TM) modes are chosen in region B. Careful examination of the inner product terms $\langle \hat{E}_j, \hat{e}_i \rangle$ and $\langle \hat{H}_j, \hat{h}_i \rangle$ given in the Appendix show that the matrix elements in (5) are either real or imaginary depending on whether the region A waveguide modes or the dielectric-loaded (region B) waveguide modes are propagating or cut off. The structure of the matrix is such that a given row, or column, is either real or imaginary. Thus, by proper multiplication of all the elements of certain rows (and columns) by j, the matrix can be transformed to a real matrix without changing the value of its determinant. This property has been exploited to advantage in eliminating the need to numerically calculate the value of complex determinants, and only numerical calculations of real determinants are needed.

III. Mode Classification

Resonant modes in dielectric-loaded resonators are more complicated to designate than in homogeneously filled resonators. Kobayashi [15] has proposed a mode designation that distinguishes the modes as EH and HE to identify the nature of the hybrid modes as having strong axial magnetic or electric fields, respectively. In this paper we introduce a different but somewhat simpler scheme.

The modes will be designated as HEH_{nm}, HEE_{nm}, TEH_{0m}, TEE_{0m}, TMH_{0m}, or TME_{0m}. The first two letters indicate whether the modes are hybrid (HE), transverse electric (TE) or transverse magnetic (TM). The third letter (E or H) indicates whether the symmetry plane $z = 0$ is an electric wall or magnetic wall, respectively. The first subscript n indicates the order of the angular or ϕ variation of the fields ($\cos n\phi$ and $\sin n\phi$). Notice that $n = 0$ for all the TE and TM modes. The second subscript m is the order of the resonant frequency, $m = 1$ being the lowest resonant of the particular mode with angular variation $\cos n\phi$ and $\sin n\phi$. Note that this designation does not indicate the radial (r) nor the axial (z) field variations. It merely orders the modes according to their resonant frequency.

This mode designation scheme has several advantages that, to some degree, help in practical applications. As will be seen in Section IV below, since generally no single mode of the infinite dielectric-loaded waveguide dominates the resonators field, it is apparent that there is no direct correlation between the two. Furthermore, indication of the type of symmetry in the mode designation helps in the determination of the possible methods that could be used in exciting the resonant mode in its symmetry plane (e.g., an axial probe could not be used to excite an HEE mode at the center of the resonator). Finally, it is noticed that the commonly used third index (usually referred to as δ) is not needed in the present mode designation scheme. This is because the ordering of the modes by the second subscript (m) in accordance with their frequency eliminates the need for this third subscript.

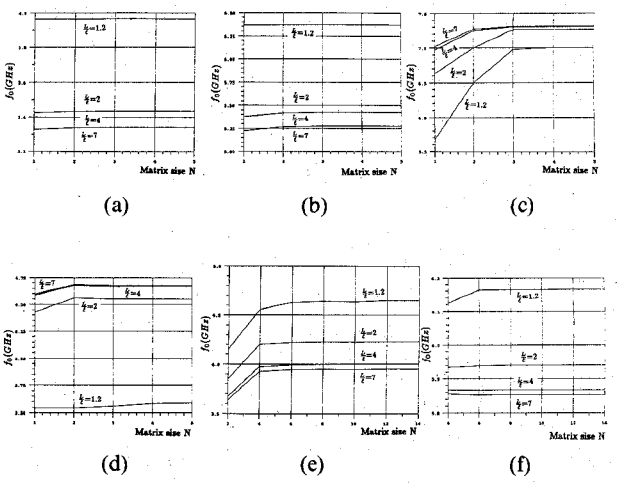

Fig. 2. Convergence test of resonant frequency as a function of matrix size m. $\epsilon_{r_1} = 35.74$, $a = 0.34$ in, $l = 0.3$ in, $b = 0.57$ in. (a) TEH_{01} mode. (b) TEE_{01} mode. (c) TMH_{01} mode. (d) TME_{01} mode. (e) HEH_{11} mode. (f) HEE_{11} mode.

IV. Results

A computer program for the calculation of the resonant frequencies, mode coefficients, and field distribution in the resonators was implemented. The program was tested and, as shown later, verification of its results by extensive experimental measurements on typical resonators showed excellent agreement.

Convergence of the results as a function of the matrix size (N) (i.e., number of modes) was tested for various modes and resonator parameters. Fig. 2 shows some results of the convergence tests. The dielectric resonator used has $\epsilon_{r_1} = 35.74$, radius $a = 0.34$ in and $l = 0.3$ in. The conducting enclosure has radius $b = 0.51$ in and its length L was varied as the parameter (L/l). Generally, the axially symmetric modes TEH_{0m}, TMH_{0m}, TEE_{0m}, and TME_{0m} have the fastest convergence, requiring only 2 to 4 terms; the HEH and HEE modes requiring 6 to 8 terms for convergence. The convergence criterion employed in the computation is that the value of the resonant frequency changes by less than 0.1 percent when the matrix size is increased by two. These results are consistent with the trend found by using the method described by Kobayashi [15]. For small values of (b/a), considerably smaller number of terms are required for convergence by the present method, while for small values of (l/L), Kobayashi's method may require comparable or smaller number of terms.

A mode chart for a representative resonator is shown in Fig. 3. This chart gives the computed and measured resonant frequencies shown as stars and triangles of various modes as a function of the ratio (L/l). The measurements were made using the same dielectric rod having $\epsilon_{r_1} = 35.74$, $a = 0.34$ in, and $l = 0.30$ in, and six different enclosures all

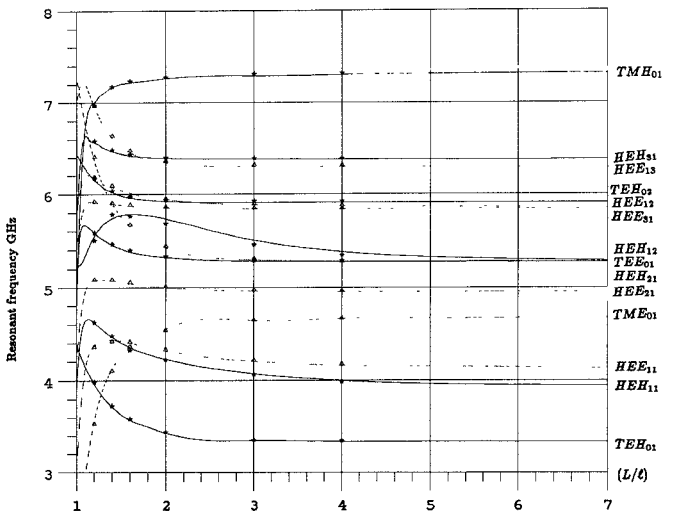

Fig. 3. Calculated and measured "Mode Chart" of dielectric-loaded resonator. $\epsilon_{r_1} = 35.74$, $a = 0.34$ in, $l = 0.3$ in, $b = 0.57$ in.

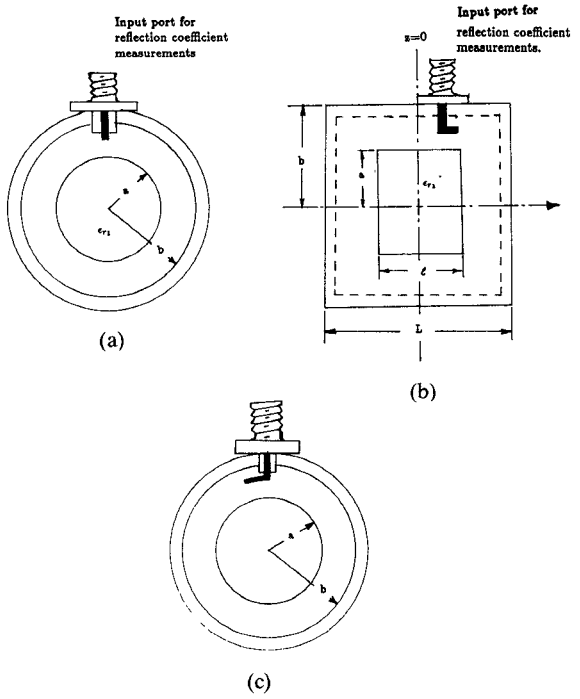

Fig. 4. Method of coupling to measure resonant frequencies of various modes. (a) Coupling coaxial probe to radial electric field (ϵ_r) TMH_{0n} and HEH_{mn} modes. (b) Coupling coaxial probe to axial electric field (H_z) TME_{0n} and HEE_{nm} modes. (c) Coupling coaxial probe to angular electric field (E_ϕ) TEE_{0n} and TEH_{0n} modes.

with the same radius $b = 0.51$ in and variable lengths L. The resonant frequency measurement and mode identification was made by lightly coupling a coaxial probe located at either the center or slightly offset from center, to the radial, the axial, or the angular electric fields of the modes as shown in Fig. 4. To ensure accuracy, the probe's length was adjusted so that at resonance, the input reflection coefficient for the mode being measured was less than -20 dB. With the exception of the HEH_{12} mode, all the measured and computed results are within less than ± 0.5 percent from each other.

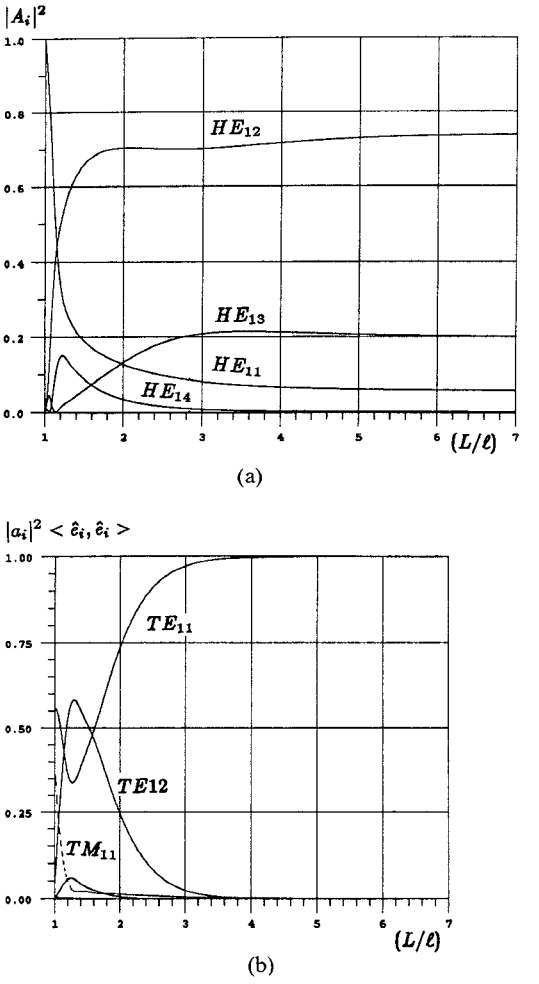

Fig. 5. Mode expansion coefficients for HEH_{11} resonant mode. (a) Dielectric-loaded region. (b) End regions.

The mode expansion coefficients in the dielectric-loaded region (A_i's) and in the end regions (a_i's) have been computed by solving (N-1) equations of the homogeneous system of (4) and normalizing the A_i, coefficients such that

$$\sum_{i=1}^{N} A_i^2 = 1. \tag{7a}$$

Although with this normalization the a_i's are uniquely determined, in order to give indication of the relative energy stored in the fields of the corresponding modes, the a_i's have been renormalized independently such that

$$\sum_{i=1}^{N} a_i^2 < \hat{e}_i, \quad \hat{e}_i > = 1. \tag{7b}$$

Variation of A_i^2 and a_i^2 with (L/l) in resonators having the same parameters as given above, and various resonant modes are shown in Figs. 5–10. In the case of the HEH_{11} mode (Fig. 5(a)) for $(L/l) = 1$, only one hybrid mode (HE_{11}) of the dielectric-loaded waveguide exists in the structure [3]. As the enclosure length is increased, other dielectric-loaded waveguide modes are generated with the coefficient of the hybrid HE_{12} mode increasing rapidly until $(L/l) = 2$, where the HE_{12} mode accounts for about 70 percent of the total energy. For $(L/l) > 3$, the HE_{12}

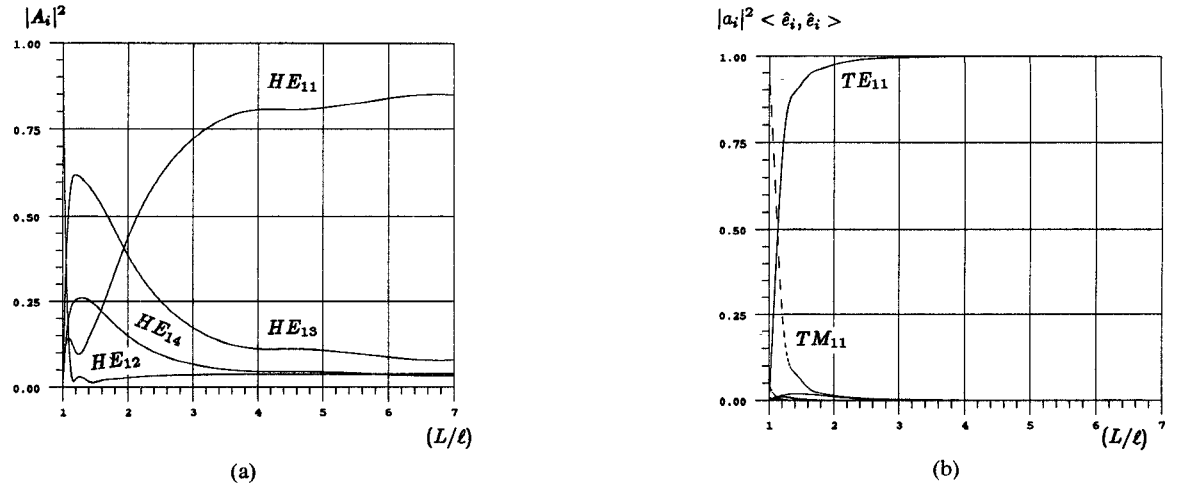

Fig. 6. Mode expansion coefficients for HEE_{11} resonant mode. (a) Dielectric-loaded region. (b) End regions.

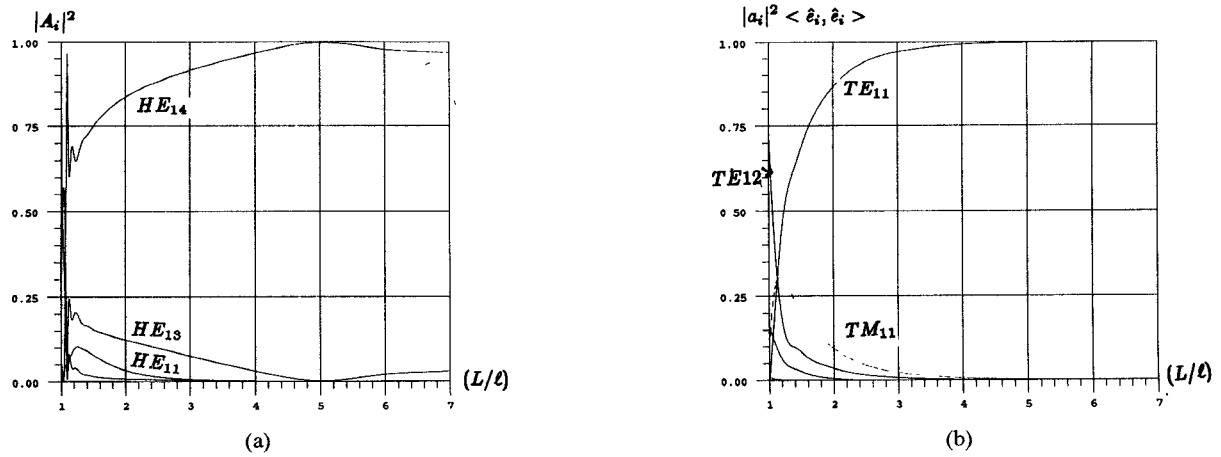

Fig. 7. Mode expansion coefficients for HEH_{12} resonant mode. (a) Dielectric-loaded region. (b) End regions.

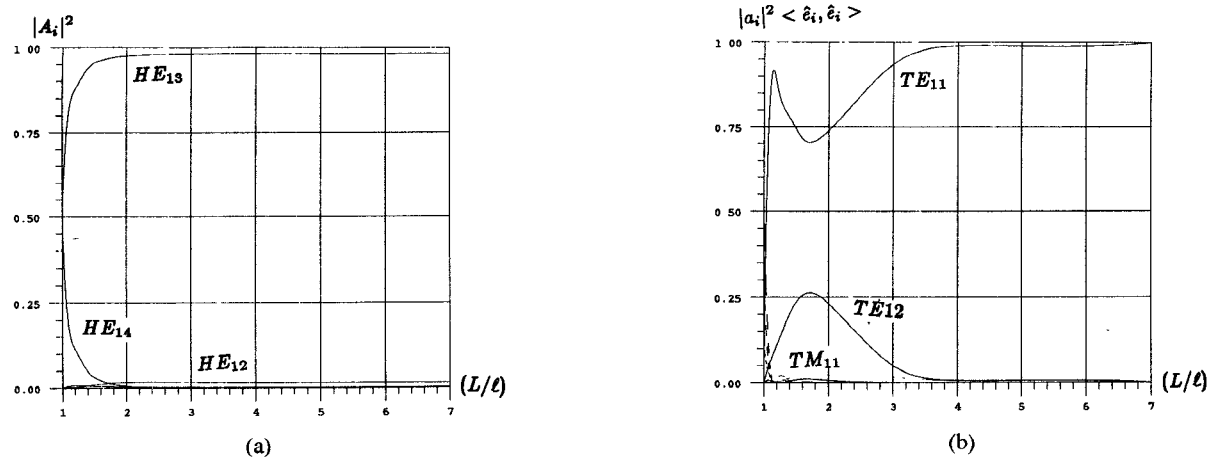

Fig. 8. Mode expansion coefficients for HEE_{12} resonant mode. (a) Dielectric-loaded region. (b) End regions.

mode dominates the fields, with the HE_{13} mode accounting for about 20 percent of the resonator's energy, and the HE_{11} mode for slightly less than 10 percent. Both the HE_{11} and HE_{12} modes in the dielectric-loaded waveguide are propagating modes at the resonant frequency of the resonator. The HE_{13} mode is cutoff. The mode expansion coefficients in the end regions shown in Fig. 5(b) have the TE_{11} mode dominating for $(L/l) > 3$. For smaller values of (L/l), significant contents of the TM_{11}, TE_{12}, and TE_{13} modes are present in addition to the TE_{11} mode. Fig. 6(a) and (b) give the mode expansion coefficients for the HEE_{11} resonant mode. In the dielectric-loaded region when (L/l)

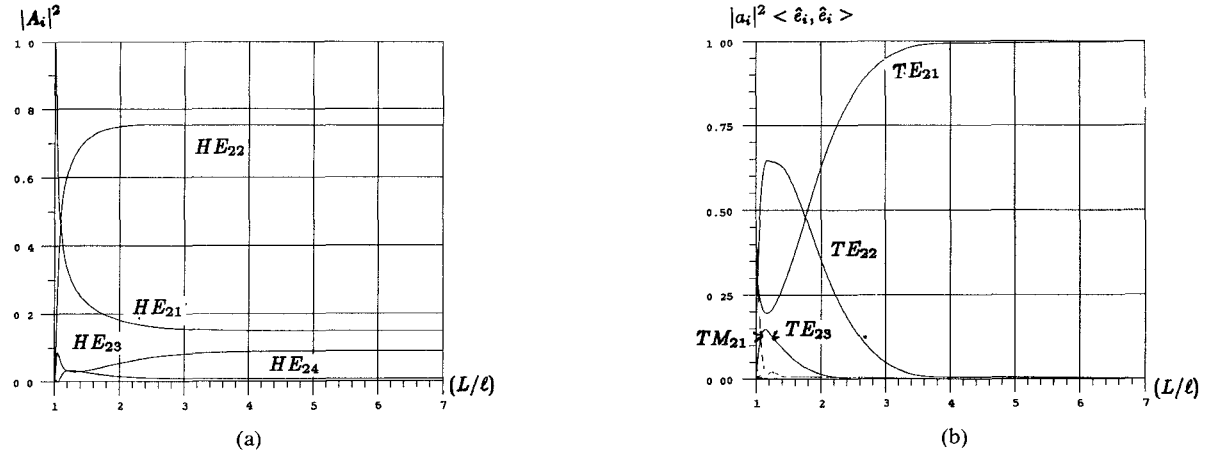

Fig. 9. Mode expansion coefficients for HEH_{21} resonant mode. (a) Dielectric-loaded region. (b) End regions.

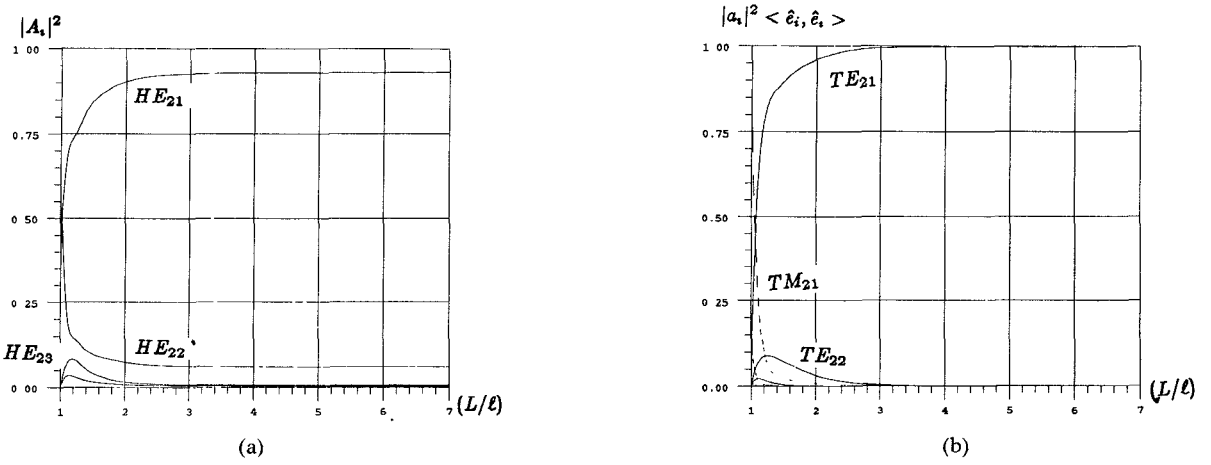

Fig. 10. Mode expansion coefficients for HEE_{21} resonant mode. (a) Dielectric-loaded region. (b) End regions.

$=1$, only the HE_{12} dielectric-loaded waveguide mode is excited. As (L/l) is increased, the HE_{12} mode coefficients reduce very rapidly, while the HE_{13} and HE_{14} mode coefficients dominate, peaking at about $(L/l) \approx 1.35$. These modes start to decay as (L/l) increases further, with the HE_{11} mode dominating for $(L/l) > 3$. In the homogeneously filled end regions, the TE_{11} mode coefficient rapidly becomes dominant as (L/l) becomes greater than about 2, as seen in Fig. 6(b). Variation of the mode expansion coefficients for the HEH_{12}, HEE_{12}, HEH_{21}, and HEE_{21} resonant modes with (L/l) are shown in Figs 7–10, respectively. As seen from these figures, the general behavior of the mode expansion is similar to that described above for the HEH_{11} and HEE_{11} resonant modes, i.e., for small values of (L/l), generally a large number of waveguide modes is needed to represent the resonant fields, but for larger values of (L/l), the mode coefficients stabilize with one waveguide mode dominating.

V. Field Computation and Plotting

The methods of numerical computation and plotting of the fields are extensions of the procedures in [2]. For a given resonant mode, the resonant frequency and expansion coefficients of the fields in terms of the normal waveguide modes are computed as described above. The angular variation of the fields in any cross section of the resonator has the same functional form (i.e. $\cos n\phi$ and $\sin n\phi$ for the HEH_{nm} and HEE_{nm} modes). Consequently, each of the radial and angular components of the fields (E_r, H_r, E_ϕ, and H_ϕ) are expressible as the product of two functions: One is a function of r only, and the other is a function of ϕ only

$$E_r = e_r(r)\sin n\phi \qquad H_r = h_r(r)\cos n\phi \tag{8}$$

$$E_\phi = e_\phi(r)\cos n\phi \qquad H_\phi = h_\phi(r)\sin n\phi. \tag{9}$$

The functions $e_r(r)$, $e_\phi(r)$, $h_r(r)$, and $h_\phi(r)$ are linear combinations of the modal functions existing in infinite dielectric-loaded (hybrid modes) or homogeneously filled waveguide (TE and TM modes), in the corresponding regions of the resonator, respectively. The resonant frequency and coefficients of the modes are obtained by solving for the roots of the determinant of a homogeneous set of linear equations (6). For efficient numerical evaluation of the fields, rather than computing four two-dimensional arrays for the values of the field components at a

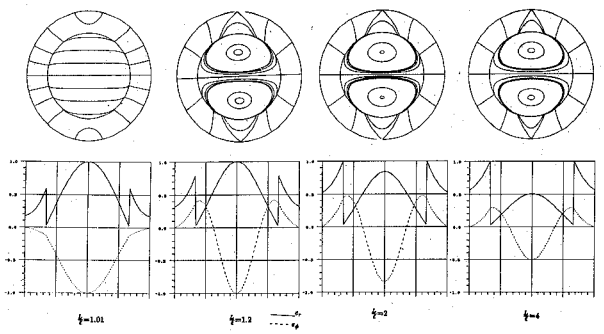

Fig. 11. Electric fields for HEH_{11} mode at $z = 0$.

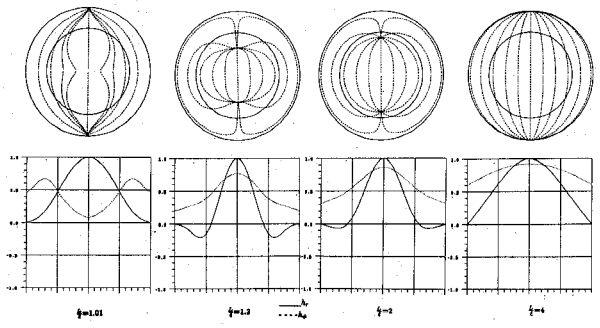

Fig. 12. Magnetic fields for HEH_{11} mode at $z = L/2$.

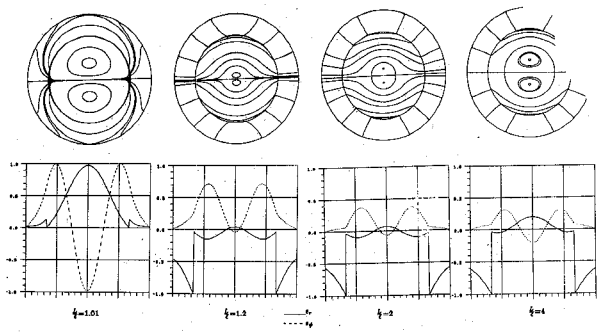

Fig. 13. Electric fields for HEH_{12} mode at $z = 0$.

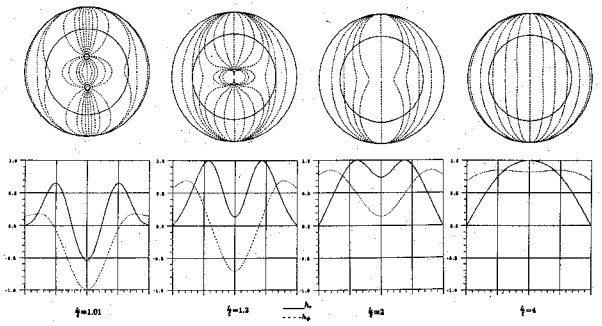

Fig. 14. Magnetic fields for HEH_{12} mode at $z = L/2$.

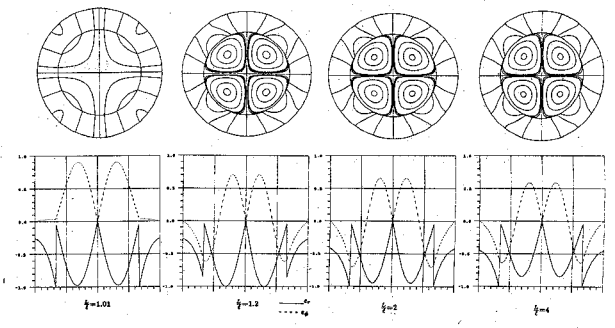

Fig. 15. Electric fields for HEH_{21} mode at $z = 0$.

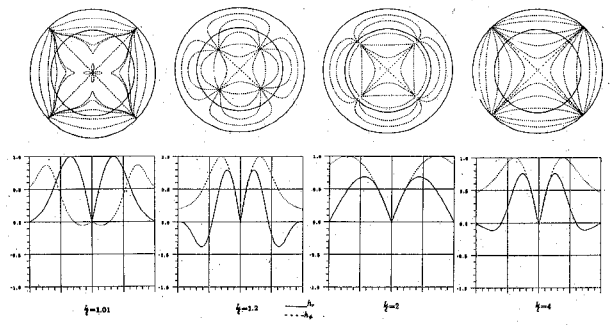

Fig. 16. Magnetic fields for HEH_{21} mode at $z = L/2$.

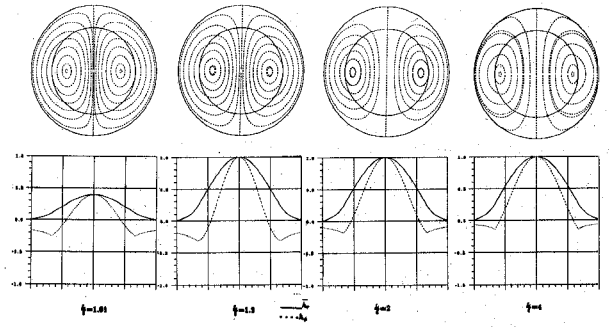

Fig. 17. Magnetic fields for HEE_{11} mode at $z = 0$.

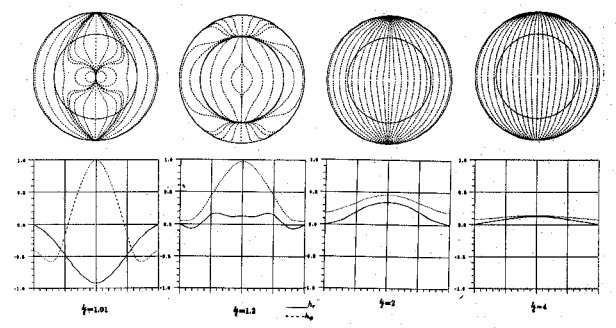

Fig. 18. Magnetic fields for HEE_{11} mode at $z = L/2$.

grid of points (r_i, ϕ_i) of the resonator cross section, only four one-dimensional arrays of the values of the functions $e_r(r)$, $e_\phi(r)$, $h_r(r)$, and $h_\phi(r)$ are computed and stored for a prescribed set of points (r_i) of the variable r. These values are subsequently used with (8) and (9) to find the fields at any point in the resonator's cross section. Electric- and magnetic-field plots are generated using the method described in [2] and [21].

Extensive computations were carried out to find the field distributions and intensity in dielectric-loaded resonators (for the first few lowest order modes). Results of these computations are presented in this section. The fields are computed and presented in two cross-sectional planes of the resonators: in the middle cross section ($z = 0$) and in the end plane ($z = L/2$). In the resonator's center plane ($z = 0$), the transverse electric-field distributions are com-

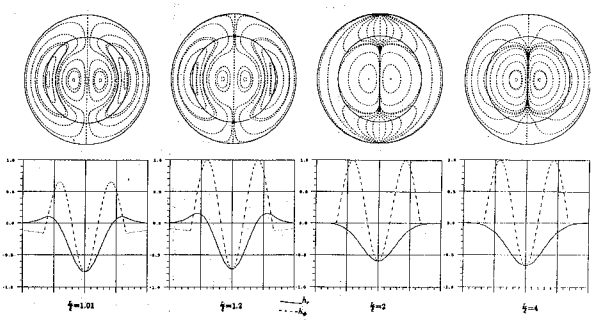

Fig. 19. Magnetic fields for HEE_{12} mode at $z = 0$.

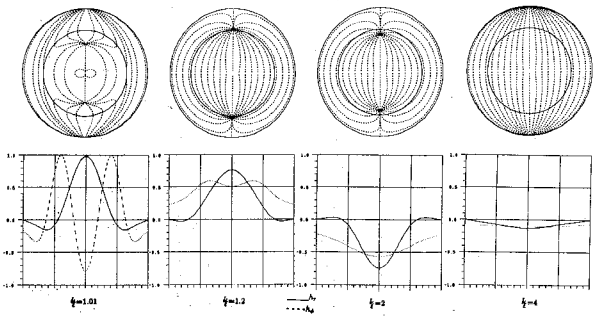

Fig. 20. Magnetic fields for HEE_{12} mode at $z = L/2$.

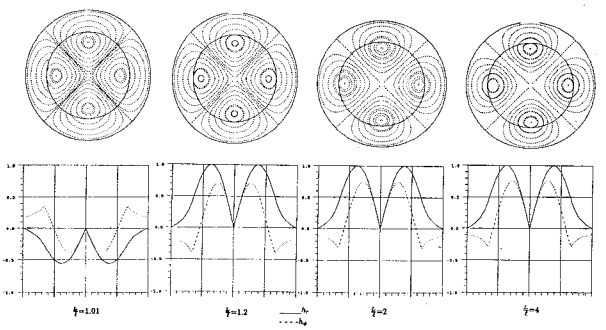

Fig. 21. Magnetic fields for HEE_{21} mode at $z = 0$.

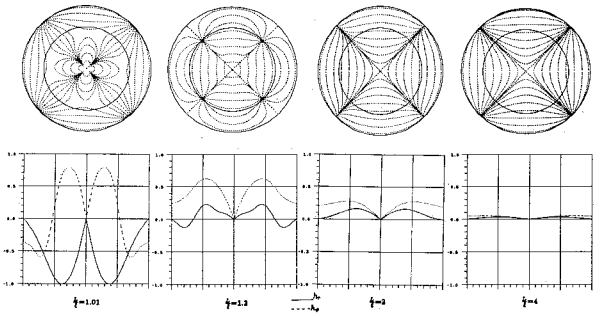

Fig. 22. Magnetic fields for HEE_{21} mode at $z = L/2$.

puted and presented for the HEH, TMH, and TEH modes (i.e., magnetic wall boundary condition), since for these modes the transverse magnetic fields vanish at $z = 0$. Similarly, the transverse magnetic fields are computed and presented in the plane $z = 0$ for the HEE, TME, and TEE modes (i.e., electric wall boundary condition), since for these modes the transverse electric fields are zero. On the end plane ($z = L/2$), the tangential electric fields vanish for all the modes, and hence only magnetic-field distributions are presented. The field plots are shown in Figs. 11–22. The common parameters used to generate these plots are

relative dielectric constant of the resonator-$\epsilon_{r_1} = 35.74$,
radius of the conducting enclosure $b = 0.57$ in,
radius of the dielectric resonator $a = 0.34$ in,
length of the dielectric resonator $l = 0.300$ in.

In each of the figures, the effect of varying the enclosure length L on the field distributions is shown by displaying these distributions for four different values of the ratio (L/l) i.e., $(L/l) = 1.01$, 1.2, 2.0, and 4.0. The field intensity (i.e., the functions e_r, e_ϕ, h_r, and h_ϕ of (9) and (10)) are shown as a function of r. The field lines in the resonator's cross section are shown only for the nonaxially symmetric modes (i.e., HEH and HEE modes), since for the TE and TM modes these field lines consist of circles and radii.

The general behavior of the field distributions can be qualitatively described by considering the variation of the mode expansion coefficients presented in Section IV, as a function of (L/l). For values of (L/l) very close to unity $(L/l = 1.01)$, the fields in the resonator's section very closely resemble the fields of a single mode existing in an infinite dielectric-loaded waveguide [2]. This is seen, for example in Figs. 11, 13, and 15 where the electric-field distributions for $(L/l) = 1.01$ cases are identical in shape to the HE_{11}, HE_{12} and HE_{21} waveguide hybrid mode fields, respectively. For a slight increase in the value of (L/l), the field structure in the center of the resonator changes rapidly. Significant contents of the other dielectric-loaded waveguide hybrid modes start to be generated, resulting in a dramatic change in the composite field distributions from the initial shape. Further increase in the ratio (L/l) results in a "stabilization" of the fields with a single hybrid waveguide mode dominating. This mode is generally different from the initial mode that existed for (L/l) ratio close to unity. This "transitional mode" effect is again seen, for example, in Figs. 11, 13, and 15, as the (L/l) ratio increases from 1.2 to 2 to 4, the initial field distributions of the hybrid mode fields HE_{11}, HE_{12}, and HE_{21} tend to the final distributions of the hybrid mode fields HE_{12}, HE_{14}, and HE_{22}, respectively, In the homogeneously filled end regions for values of $(L/l) = 1.01$, the magnetic fields in the end plane $z = L/2$ have a relatively large number of the normal waveguide modes (TE and TM). As (L/l) is increased, some of these modes become less pronounced and the end region fields tend to a single dominating normal mode. This is seen in Figs 12, 14, and 16 where the magnetic field lines in the end planes $z = L/2$ are shown for various values of (L/l) for the HEH_{11}, HEH_{12}, and HEH_{21} modes, respectively. Clearly for $(L/l) = 1.01$, 1.2, and 2, no single mode is dominant as can be seen from the field lines. For $(L/l) = 4$, these magnetic fields have the same distribution as TE_{11}, TE_{11}, and TE_{21}

normal modes in the homogeneously filled waveguide, respectively.

The field distributions for HEE modes generally behave in a similar way to that described above for the HEH modes, except that in the center $z = 0$, the magnetic fields appear to be less sensitive to variations in the ratio (L/l). This can be seen from Figs. 17, 19, and 21 which show magnetic-field distribution in the plane $z = 0$ for the HEE_{11}, HEE_{12}, and HEE_{21} modes, respectively. Fields in the end plane $z = L/2$ for these modes are shown in Figs. 18, 20, and 22, and for large values of (L/l), the field distributions tend to the TE_{11}, TE_{11}, and TE_{21} modes for the homogeneously filled waveguide, respectively.

VI. Conclusions and Discussions

The method of analysis presented in this paper leads to the complete accurate determination of the fields and resonant frequencies of dielectric-loaded resonators. Compared to the method developed by Kobayashi [15], the present method has much faster convergence properties for small (b/a), and gives a representation of the fields in the resonator in terms of dielectric loaded or homogeneously filled identifiable waveguide modes. The mode designation scheme proposed in this paper is a simple and logical way of identifying the various resonances, and gives useful insight into the physical structure of the fields, which in turn helps in practical application of this type of resonators. The mode coefficients indicate that for practical resonator dimensions no single dielectric waveguide mode is dominant. Experimental results of the resonators mode chart showed excellent agreement with the calculations.

The field plots presented are useful qualitative tools that pictorially display the field structures for the resonant modes in dielectric-loaded resonators. They can help in the design of devices using these types of resonators by indicating locations of strong fields, their directions, etc.

It is seen that the spacing between the conducting enclosure's end planes and the dielectric material (or the ratio L/l) has a pronounced effect on the mode contents of the fields. When this ratio is large, the field distributions in the dielectric-loaded region and in the homogeneously filled end regions are representable by a single mode of the corresponding waveguide. Magnetic-field distributions in the end planes of the enclosure provide useful information on how to couple two such resonators together or excite the required modes.

Appendix
Analytic Expressions for the Inner Products

In the following expressions, k_c represents the cutoff wavenumbers of either a TE or TM mode in a circular waveguide of radius b and full of a dielectric material of relative permittivity ϵ_{r_3}, Γ_{HE_i} are roots of the characteristic equation for an infinite length dielectric-loaded waveguide. Equation (13) in [2], P_n and R_n are defined by (10) and (11) of [2].

$$\frac{\langle \hat{E}_{HE_i}, \hat{e}_{TE_j} \rangle}{\langle \hat{e}_{TE_j}, \hat{e}_{TE_j} \rangle} = \frac{-jk_c^2 \Gamma_{HE_i}}{\omega \mu I_{TE_j}} [A + \alpha(B + C)]$$

$$\frac{\langle \hat{H}_{HE_i}, \hat{h}_{TE_j} \rangle}{\langle \hat{h}_{TE_j}, \hat{h}_{TE_j} \rangle} = \frac{jk_c^2}{\omega \mu \gamma_{TE_j} I_{TE_j}} \left[nJ_n(\xi_1 a) J_n(k_c a) \cdot \left(\frac{k_1^2}{\xi_1^2} + \frac{k_2^2}{\zeta_2^2} \right) - \alpha \Gamma_{HE_i}^2 (B + C) \right]$$

$$\frac{\langle \hat{E}_{HE_i}, \hat{e}_{TM_j} \rangle}{\langle \hat{e}_{TM_j}, \hat{e}_{TM_j} \rangle} = \frac{k_c^2 \Gamma_{HE_i}}{\gamma_{TM_j} I_{TM_j}} [\alpha A + B + D]$$

$$\frac{\langle \hat{H}_{HE_i}, \hat{h}_{TM_j} \rangle}{\langle \hat{h}_{TM_j}, \hat{h}_{TM_j} \rangle} = \frac{k_c^2}{\omega^2 \mu \epsilon_3 I_{TM_j}} \left[-\alpha \Gamma_{HE_i}^2 A + k_1^2 B + k_2^2 D) \right]$$

$$\frac{\langle \hat{E}_{TE_i}, \hat{e}_{TE_j} \rangle}{\langle \hat{e}_{TE_j}, \hat{e}_{TE_j} \rangle} = \frac{k_c^2 (B + C)}{I_{TE_j}}$$

$$\frac{\langle \hat{H}_{TE_i}, \hat{h}_{TE_j} \rangle}{\langle \hat{h}_{TE_j}, \hat{h}_{TE_j} \rangle} = \frac{k_c^2 \Gamma_{TE_i}}{\gamma_{TE_j}} \frac{(B + C)}{I_{TE_j}}$$

$$\frac{\langle \hat{E}_{TM_i}, \hat{e}_{TM_j} \rangle}{\langle \hat{e}_{TM_j}, \hat{e}_{TM_j} \rangle} = \frac{k_c^2 \Gamma_{TM_i}}{\gamma_{TM_j}} \frac{(B + D)}{I_{TM_j}}$$

$$\frac{\langle \hat{H}_{TM_i}, \hat{e}_{TM_j} \rangle}{\langle \hat{h}_{TM_j}, \hat{h}_{TM_j} \rangle} = \frac{k_c^2}{\epsilon_{r_3}} \frac{(\epsilon_1 B + \epsilon_2 D)}{I_{TM_j}}$$

where

$$I_{TE_j} = \frac{1}{2}(k_c^2 b^2 - n^2) J_n^2(k_c b)$$

$$I_{TM_j} = \frac{k_c^2 b^2}{2} J_{n-1}^2(k_c b) = \frac{k_c^2 b^2}{2} J_n'^2(k_c b)$$

$$A = n \left(\frac{1}{\xi_1^2} + \frac{1}{\zeta_2^2} \right) J_n(\xi_1 a) J_n(k_c a)$$

$$B = \frac{a}{\xi_1^2} \left[\xi_1 \left(1 + \frac{\xi_1^2}{k_c^2 - \xi_1^2} \right) J_n(k_c a) J_n'(\xi_1 a) - \frac{\xi_1^2 k_c}{k_c^2 - \xi_1^2} J_n'(k_c a) J_n(\xi_1 a) \right]$$

$$C = \frac{a}{\zeta_2^2} \left[\zeta_2 \left(1 - \frac{\zeta_2^2}{k_c^2 + \zeta_2^2} \right) J_n(k_c a) P_n'(\zeta_2 a) + \frac{\zeta_2^2 k_c}{k_c^2 + \zeta_2^2} J_n'(k_c a) J_n(\xi_1 a) \right]$$

$$D = \frac{a}{\zeta_2^2} \left[\zeta_2 \left(1 - \frac{\zeta_2^2}{k_c^2 + \zeta_2^2} \right) J_n(k_c a) R_n'(\zeta_2 a) + \frac{\zeta_2^2 k_c}{k_c^2 + \zeta_2^2} J_n'(k_c a) J_n(\xi_1 a) \right].$$

REFERENCES

[1] K. A. Zaki and A. E. Atia,"Modes in dielectric-loaded waveguides and resonators," *IEEE Trans. Microwave Theory Tech.*, vol. MTT-31, pp. 1039–1045, Dec. 1983.

[2] K. A. Zaki and C. Chen,"Intensity and field distribution of hybrid modes in dielectric-loaded waveguides," *IEEE Trans. Microwave Theory Tech.*, vol. MTT-33, pp. 1442–1447, Dec. 1985.

[3] K. A. Zaki and C. Chen,"Loss mechanisms in dielectric-loaded resonators," *IEEE Trans. Microwave Theory Tech.*, vol. MTT-33, pp. 1448–1452, Dec. 1985.

[4] T. Itoh and R. Rudokas,"New method for computing the resonant frequencies of dielectric resonators," *IEEE Trans. Microwave Theory Tech.*, vol. MTT-25, pp. 52–54, Jan. 1977.

[5] A. Okaya and C. F. Barash,"The dielectric microwave resonator," *Proc. IRE*, vol. 50, pp. 2081–2092, Oct. 1962.

[6] R. De Smedt,"Correction due to a finite permittivity for a ring resonator in free space," *IEEE Trans. Microwave Theory Tech.*, vol. MTT-32, p. 1288–1293, Oct. 1984.

[7] M. Tsuji, H. Shigesawa, and K. Takiyama,"Analytical and experimental investigations on several resonant modes in open dielectric resonators," *IEEE Trans. Microwave Theory Tech.*, vol. MTT-32, pp. 628–632, June 1984.

[8] W. E. Hord and F. J. Rosenbaum,"Approximation techniques for dielectric-loaded waveguides," *IEEE Trans. Microwave Theory Tech.*, vol. MTT-16, pp. 228–233, Apr. 1968.

[9] W. J. English and F. Y. J. Young,"An E-vector variational formulation of the Maxwell equations for cylindrical waveguide problems," *IEEE Trans. Microwave Theory Tech.*, vol. MTT-19, pp. 40–46, Jan. 1971.

[10] J. Van Bladel,"High-permittivity dielectrics in waveguides and resonators," *IEEE Trans. Microwave Theory Tech.*, vol. MTT 22, pp. 32–37, Jan. 1974.

[11] A. S. Omar and K. Schunemann,"Scattering by dielectric obstacles inside guiding structures," 1984 *IEEE-MTT-S Int. Microwave Symp. Dig.*, pp. 321–323, June 1984.

[12] Y. Kobayashi and S. Tanaka,"Resonant modes of a dielectric rod resonator short circuited at both ends by parallel conducting plates," *IEEE Trans. Microwave Theory Tech.*, vol. MTT-28, pp. 1077–1085, Oct. 1980.

[13] Y. Kobayashi and M. Miura,"Optimum design of shielded dielectric rod and ring resonators for obtaining the best mode separation," *IEEE-MTT-S Int. Microwave Symp. Dig.*, pp. 184–186, June 1984.

[14] S. Maj and M. Pospieszalski,"A composite cylindrical dielectric resonator," 1984 *IEEE-MTT-S Int. Microwave Symp. Dig.*, pp. 190–192, June 1984.

[15] Y. Kobayashi, N. Fukuoka, and S. Yoshida,"Resonant modes for a shielded-dielectric rod resonator," *Elect. Commun. Japan*, vol. 64-B, 1981-translation, 1983 Scripta Publishing Co.

[16] U. S. Hong and R. H. Jansen,"Numerical analysis of shielded dielectric resonators including substrate, support disk, and tuning post," *Electron. Lett.*, vol. 18, pp. 1000–1002, Nov. 1982.

[17] D. Kajfez, A. W. Glisson, and J. James,"Computed modal-field distributions for isolated dielectric resonator," *IEEE Trans. Microwave Theory Tech.*, vol. MTT-32, pp. 1609–1616, Dec. 1984.

[18] A. W. Glisson, D. Kajfez, and J. James,"Evaluation of modes in dielectric resonators using a surface integral equation formulation," *IEEE Trans. Microwave Theory Tech.*, vol. MTT-31, pp. 1023–1029, Dec. 1983.

[19] R. E. Collin, *Field Theory of Guided Waves*, New York: McGraw-Hill, 1960, ch. 5.

[20] P. J. B. Clarricoats and B. C. Taylor,"Evanescent and propagating modes of dielectric-loaded circular waveguide," *Proc. IEE*, vol 111, pp. 1951–1956, Dec. 1964.

[21] E. R. Nagelberg and J. M. Hoffspiegel,"Computer-graphic analysis of dielectric waveguides," *IEEE Trans Microwave Theory Tech.*, vol. MTT-15, pp. 187–189, Mar. 1967.

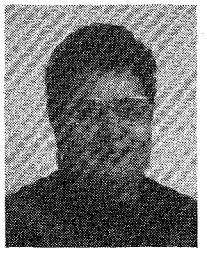

Kawthar A. Zaki (SM'85) received the B.S. degree with honors from Ain Shams University, Cairo, Egypt, in 1962, and the M.S. and Ph.D. degrees from the University of California, Berkeley, in 1966 and 1969, respectively, all in electrical engineering.

From 1962 to 1964, she was a Lecturer in the Department of Electrical Engineering, Ain Shams University. From 1965 to 1969, she held the position of Research Assistant in the Electronic Research Laboratory, University of California, Berkeley. She joined the Electrical Engineering Department, University of Maryland, College Park, MD, in 1970, where she is presently an Associate Professor. Her research interests are in the areas of electromagnetics, microwave circuits, optimization, and computer-aided design.

Dr. Zaki is a member of Tau Beta Pi.

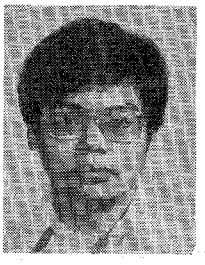

Chunming Chen (S'85) was born in Taiwan, Republic of China in 1958. He received the B.S. degree from the National Tsing Hua University, Taiwan, in 1981 and the M.S. degree from the University of Maryland, College Park, in 1985, both in electrical Engineering.

Since 1984, he has worked as a research assistant in the Department of Electrical Engineering, University of Maryland, College Park. He is now working towards the Ph.D. degree in the area of microwave components and circuits.